INTERCALATION STUDIES OF LEWIS BASES INTO LAYERED TRANSITION METAL DICHALCOGENIDES

by

Jacob Armitage, B.S.

A thesis submitted to the Graduate College of
Texas State University in partial fulfillment
of the requirements for the degree of
Master of Science
with a Major in Chemistry
May 2016

Committee Members:

Gary Beall

Todd Hudnall

Benjamin Martin

FAIR USE AND AUTHOR'S PERMISSION STATEMENT

Fair Use

Duplication Permission

ACKNOWLEDGEMENTS

I would first and foremost like to thank Dr. Benjamin Martin for his knowledge, guidance, and patience throughout my academic endeavors. The skills and experience I have gathered working with you will undoubtedly serve me throughout my career. I would also like to acknowledge my committee members: Dr. Gary Beall, Dr. Todd Hudnall, and Dr. Martin. You have all contributed to my graduate career, and have given me a high standard of professionalism and accomplishment to aspire for.

TABLE OF CONTENTS

Page

LIST OF TABLES

Table **Page**

LIST OF FIGURES

Figure **Page**

ABSTRACT

Solvation and exfoliation mechanics of layered transition metal dichalcogenides (TMDs) were studied. Lithium vanadium disulfide ($LiVS_2$) is an alkali-metal intercalate of vanadium disulfide, consisting of 2-dimensional anionic VS_2 sheets with interlayer Li cations. X-ray diffraction and potentiometric analysis shows $Li_{(1-x)}VS_2$ undergoes reversible phase changes during oxidative delithiation. An affinity for solvation of the VS_2 layers was observed for $0 < x < 0.4$ by a range of solvents, while $LiVS_2$ and fully oxidized VS_2 show little propensity for direct solvation over short time scales. Understanding the relationship between oxidation state and solvation of TMDs may lead to novel electrolyte formulations that inhibit degradation of electrochemical storage devices over multiple charge cycles. Directed tuning of the interlayer cation density in TMDs such as VS_2 may also provide a new means of soft chemical exfoliation and generation of pristine two-dimensional crystalline materials.

I. INTRODUCTION

Layered materials have been the focus of study for several decades due to their unique physical and chemical properties[1] and the field has been invigorated by the isolation and numerous applications of monolayer graphene.[2] These materials can be best described as stacked two-dimensional crystals, where the principle layers of the bulk material consist of covalent or coordination-bonded planes. Individual layer morphology is diverse and may consist of single atomic planes, such as in graphite or boron nitride, or several stacked close-packed layers. Modern applications for these materials include sensing and microelectronics[3], electrochemical energy storage[45], and catalytic alternatives to rare-earth metals.[6,7] Their utility may depend on the layered morphology of the bulk compound, or on properties of exfoliated 2D monolayers.

The first commercially successful rechargeable lithium ion batteries incorporated lithium cobalt oxide ($LiCoO_2$) as a cathode material.[8] In this compound, cobalt is octahedrally coordinated between parallel planes of oxygen atoms, forming CoO_2 sandwich layers. Lithium cations which inhabit octahedral sites in the interlayer gallery of this compound are mobile and allow for topotactic ion exchange chemistry. Lithium ion batteries employing $LiCoO_2$ exhibit high energy density, although they are prone to degradation over repeated cycling and are relatively expensive to produce. Pioneering work by John Goodenough, et al. found that carefully selecting the electrolyte composition could vastly improve the stability of some electrochemical systems.[4] These findings warrant further investigation of novel electrolyte formulations that may benefit current battery electrode characteristics.

The suitability of these compounds for electrochemical storage lies in their ability to exist as a solid solution, where the mobile charge carriers are able to reversibly intercalate the layers without significantly altering the bulk crystallinity. The theoretical capacity of a given electrochemical system is directly related to the stoichiometric range in which these solid solutions are reversibly stable. Strategies to improve battery electrode performance have been studied involving the use of mixed-metal systems, but these often have drawbacks relating to cost and abundance of required materials. The ideal formulation of an energy dense, inexpensive, simple and robust electrochemical system remains elusive, but research into layered sulfides has shown promise. There is ongoing research with transition metal dichalcogenides (TMDs), which consist of 'sandwich' layers where metal atoms can be octahedrally or tetrahedrally coordinated between sulfur planes. Many of these TMDs, including MoS_2, TiS_2, and VS_2 are redox active and can form alkali-metal intercalates. These layered TMDs offer many potential advantages for use in electrochemical storage devices, as well as being relatively inexpensive to produce.

Second to graphene, molybdenum disulfide (MoS_2) is arguably the most ubiquitous two-dimensional material currently being studied. MoS_2 has been used commercially for many years, most notably as a high temperature lubricant and also as a catalyst for hydrodesulfurization in the petrochemical industry. MoS_2 is isostructural to CoS_2 with layers consisting of molybdenum atoms coordinated in trigonal prismatic geometry between parallel sulfur planes. The structure of MoS_2 is given in Figure 1. Intercalation compounds such as $LiMoS_2$ are formed by guest species occupying the interlayer space between adjacent sulfur planes. Organolithium reagents such as

n-butyllithium are often used in this reaction. $LiMoS_2$ is unique in that it will readily exfoliate in water, forming aqueous suspensions of MoS_2 monolayers.[9]

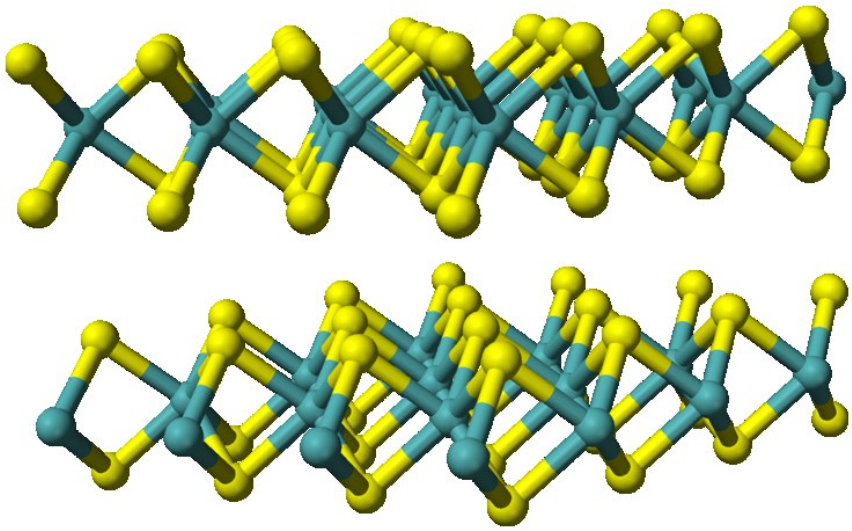

Figure 1. Ball and stick projection of 2H-MoS_2. Molybdenum atoms (light blue) are coordinated between planes of sulfur atoms. The coordination sphere in this structure is trigonal prismatic, with each molybdenum atom surrounded by six sulfur atoms, with each sulfur atom in turn sharing three molybdenum atoms.

Alkali-metal intercalates of vanadium disulfide (VS_2) and lithium vanadium diselenide (VSe_2) have also been investigated as possible cathode materials.[10,11,12] These materials share the same crystalline structure, having vanadium atoms coordinated between hexagonal close-packed layers of sulfur or selenium. The structure of $LiVS_2$ is given in Figure 2, which illustrates the VS_2 slabs intercalated by lithium cations. Many other intercalated phases of metal dichalcogenides have been studied, including amine-intercalated $LiVSe_2$[13] and a variety of TMDs intercalated by cobaltocene.[14]

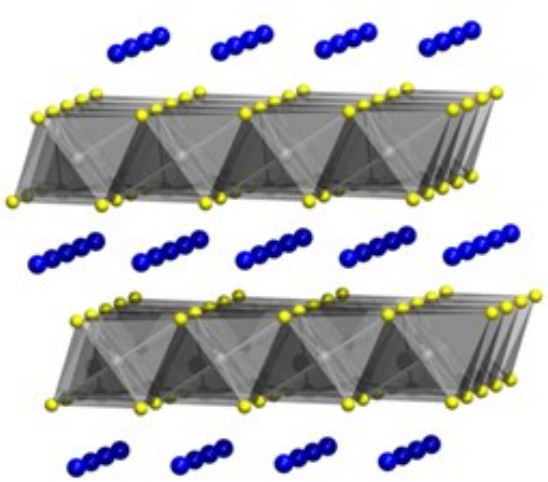

Figure 2. Crystalline structure diagram of $LiVS_2$. VS_2 layers shown as shaded grey slabs with lithium cations occupying octahedral holes in the interlayer gallery.

Layered TMDs and layered materials in general represent a largely unexplored pool of two-dimensional materials for study.[15,16] Since the isolation of monolayer graphene in 2004[17] interest has steadily grown in ways to isolate two-dimensional crystals from other layered systems. Current methods for production include growth of monolayers on a substrate using chemical vapor deposition (CVD) and solvent assisted exfoliation of bulk materials. Solvent exfoliation methods are currently the most effective means of generating large quantities of monolayer materials. The major drawback in using solvent exfoliation is that dispersion typically requires multiple sonication and centrifugation steps, often yielding high-defect monolayers.

It may be possible to modify the bulk materials to facilitate exfoliation. As shown in this work, studies of $Li_{1-x}VS_2$ indicate a nonlinear relationship between lithium ion removal and interlayer spacing, which warrants further exploration of this and other layered systems. To date, no comprehensive review of the relationship between ion content, solvation, and exfoliation characteristics in TMDs has been published. The

present research is focused primarily on studying tunable ion contents in TMDs to assist with the study of exfoliation methods and electrochemical storage applications.

II. STATEMENT OF PURPOSE

Currently many high-performance battery technologies rely on some form of topotactic ion exchange chemistry, where mobile cations or anions are intercalated or exchanged between electrodes, almost invariably requiring a solvent to facilitate ion mobility. The choice of solvents in these applications is critical and can have dramatic effects on the stability and electrochemical capacity of a given system. Many layered materials have been shown to intercalate a number of solvent species under specific conditions, which can have implications for a wide range of applications relying on current and future topotactic ion exchange chemistries. To date, no comprehensive study has been made on how the extent of oxidation of a layered chalcogenide compound affects the extent of solvation by a coordinating solvent. The purpose of this research is to: 1) study the relationship between the extent of oxidation of a layered compound and its propensity for intercalation by a coordinating Lewis base, and 2) investigate how structural differences of a coordinating base may impact its ability to intercalate a partially oxidized layered compound.

III. METHODS

Materials.

Crystalline iodine (99.5%), lithium foil (99.9%), synthetic graphite (325 mesh, 99.9995%), poly(vinylidene fluoride) powder, lithium perchlorate (99%), and sulfur (325 mesh, 99.5%) were purchased from Alfa Aesar and used as received. Liquid ammonia was dehydrated by distillation over sodium in an inert atmosphere immediately before use. Acetonitrile (anhydrous, 99.5%), formamide (99%), N-methylformamide (99%), and N,N-dimethylformamide (99.8%) were purchased from Alfa Aesar and used as received. Jeffamine EDR-148 (triethylene glycol diamine, 100.0%) was purchased from Huntsman and used as received. Hexane (anhydrous, 99.9%) was purchased from Acros Organics and used as received. Ethylene carbonate (anhydrous, 99%) and diethyl carbonate (anhydrous, ≥ 99%) were purchased from Sigma Aldrich and used as received. Hexylamine (> 99%) and 1-aminodecane (> 98%) were purchased from TCI and used as received. Vanadium powder (99.5%) was purchased from Strem Chemicals and used as received. Alkali metal sulfides (Li_2S, Li_2S_2) were synthesized by reacting stoichiometric amounts of elements in liquid ammonia on a Schlenck line.

Synthesis.

All reactants were handled in an argon filled dry box to prevent air oxidation and contamination of starting materials.

$Li_{1-x}VS_2$: In a typical synthesis, lithium sulfide (Li_2S, Li_2S_2), vanadium, and sulfur were combined in a stoichiometric ratio of 1:1:2.5 for Li:V:S (excess sulfur added as a flux) and intimately mixed by grinding in a ceramic mortar. Masses were scaled to

yield 1-2 grams total reactant mixture. The mixture was sealed within carbon-coated silica ampoules under vacuum (10^{-5} mbar). The sealed ampoules were then heated to 650 °C in a three step process consisting of 12 hour ramp, dwell, and cooling periods. The ampoules were then opened in an argon atmosphere, yielding grey-black pellets which were thoroughly ground to produce a homogenous, dark grey powder. The stoichiometric lithium content of the product was determined electrochemically.

Li_xVS_2 ($0.95 < x < 1$): Fully lithiated $LiVS_2$ was synthesized by stirring previously synthesized $Li_{1-x}VS_2$ samples in a stoichiometric excess of 2.2 M Bu-Li in hexane for 24-72 hours. After reacting, a small amount of white impurity presumed to be hydrocarbon byproducts of the hexane solvent was present in the product. This impurity was washed with anhydrous hexane and centrifuged until no visual impurities were observed. As a result of this additional wash, a large portion of the $LiVS_2$ 'silt' was removed from the top layer after centrifugation. Lithium content of the reduced $LiVS_2$ product was determined electrochemically.

$Li_{1-x}VS_2$ samples ($0 \leq x < 1$): Samples were prepared by chemical oxidation with solutions of iodine dissolved in acetonitrile. Reactions were carried out on a Schlenck line kept under positive argon pressure to mitigate possible air oxidation. To produce samples with specific lithium content, a stoichiometric amount of iodine was dissolved in acetonitrile and introduced drop-wise via syringe through a rubber septum attached to the reaction flask. The iodine solution was added slowly in this manner to prevent non-homogenous oxidation of samples. The reactions were monitored visually by iodine color dissipation, as small additions imparted a green hue to the reaction mixture which faded as iodine was consumed. Oxidized samples prepared thus were stored in

acetonitrile until used further. A sufficient mass of at least 100 mg of each oxidized sample was prepared from reduced $LiVS_2$.

Solvated Li_xVS_2: Chemical oxidation of $LiVS_2$ allowed for repeatable preparation of various $Li_{1-x}VS_2$ phases. Acetonitrile being relatively volatile allowed for easy removal after a given reaction. $Li_{1-x}VS_2$ samples were individually exposed to a selected group of primary alkyl amines and N-methyl amides (N=0, 1, 2). Powder samples were dried on a silicon disk and exposed to a solvent in an argon dry box, then sealed from atmosphere with polyamide adhesive tape. This ensured the sample remained wetted by the solvent and minimized exposure to atmosphere during analysis. Solvation was evidenced as both an interlayer expansion of the $Li_{1-x}VS_2$ and appearance of new low-angle peaks measured by powder X-ray diffraction.

Measurement.

Powder X-ray diffraction (XRD) data was collected using a Bruker D8 Focus diffractometer equipped with a Sol-X detector and a Bruker D8 Advance Eco. The detector was tuned to eliminate sample fluorescence and Cu-K□ radiation. Samples were spread thinly over a 'zero diffraction' silicon plate and protected from atmosphere using an attachable polymer dome or polyamide adhesive tape. Data was collected at ambient temperature over various ranges in the interval of 1.5 - 60° 2θ with a maximum step size of 0.06° and an integration time of no less than 4 seconds per step.

Electrochemistry.

Cyclic voltammetry and chronopotentiometry measurements were performed in an argon-filled glove box equipped with coaxial feed-through using a Gamry PCI-350

potentiostat. Working electrodes were prepared by grinding the active material, high-purity graphite, and PVDF in a 70:20:10 mass ratio with a 1:1 mixture of ethylene carbonate (EC) and diethyl carbonate (DEC) to form a paste. This paste was spread on the top face of a weighed stainless steel cylinder and vacuum dried in the dry box airlock to cast the polymer into an adherent film. The electrode was again weighed to determine dry electrode mass and attached to a Teflon base. Two glass fiber disks were sandwiched between this working electrode and the counter/reference electrode, which consisted of a clean piece of lithium foil pressed on to a second steel cylinder. The fiber disks were saturated with a 1 M $LiClO_4$ 1:1 EC:DEC electrolyte. A Teflon sleeve was used to keep the electrodes in place, with leads securely attached to each threaded electrode base. Paraffin wax film was used to seal the exterior of each cell to prevent electrolyte evaporation. Prior to running each measurement, the open circuit potential (OCP) was monitored over a period of several hours to determine stability.

IV. INITIAL STUDY AND FRACTIONAL OXIDATION OF $LiVS_2$

Our original interest was in exploring "soft" chemical routes to facilitate spontaneous exfoliation of layered materials. The exfoliation of MoS_2 has been well studied and provides a means of generating mono and few-layered nanoscale MoS_2 particles of various size distributions.[18] $LiVS_2$ was chosen as a model compound for study based on exhibiting repeatable electrochemical cycling and having chemical and physical properties similar to other more studied TMDs such as MoS_2. More recently, several methods of inducing exfoliation of layered materials have been put forward, though these methods generally rely on forced mechanical cleavage through sonication. Few examples have been found of spontaneous exfoliation similar to that seen through lithiated MoS_2, which seems to be driven in part by the solvation of interlayer cations in water.

The stability of $LiVS_2$ during redox processes was most important to our studies, as earlier attempts towards exfoliating a similar layered sulfide $NaLiCoS_2$ were unsuccessful. The crystalline structure of $NaLiCoS_2$ is similar to $LiVS_2$, however the alternating layers are composed of mixed Li/Co between pseudo close-packed sulfur layers (see Figure 3), with sodium cations occupying the octahedral sites between layers. It was expected that this compound may spontaneously exfoliate under suitable conditions, leaving free-standing $LiCoS_2$ monolayers in suspension.

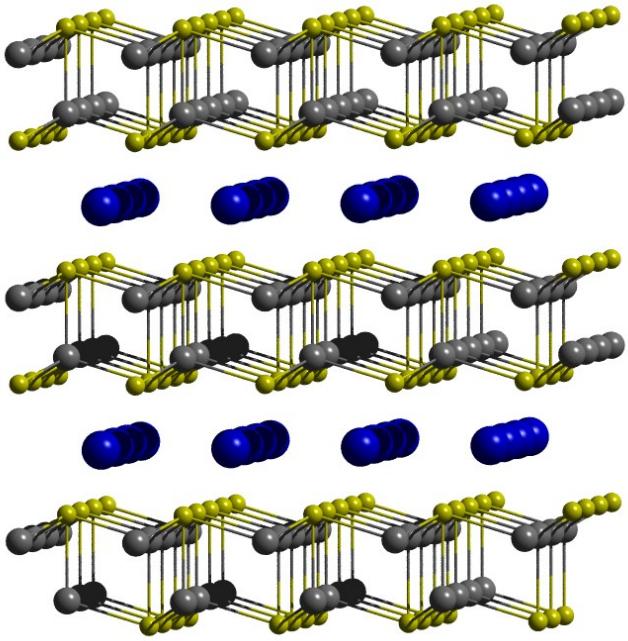

Figure 3. Crystalline structure diagram of $NaLiCoS_2$. Layers are comprised of a random 1:1 distribution of lithium/cobalt atoms tetragonally coordinated to sulfur. Sodium cations occupy the interlayer space between adjacent sulfur planes.

Electrochemical probing of $NaLiCoS_2$ showed continuous oxidation did not induce phase changes, suggesting the crystalline layered structure was preserved during oxidative deintercalation of sodium cations. It was later discovered that chemical oxidation resulted in degradation of the crystalline structure, precluding the possibility of bulk exfoliation and further study of $NaLiCoS_2$ nanoparticles by this method. XRD patterns for $NaLiCoS_2$ are given in Figure 4, showing a gradual disappearance of crystallinity relative to oxidation of the compound. Crystalline phases were not observed in fully oxidized samples, but amorphous products could be recrystallized for analysis by high temperature annealing.

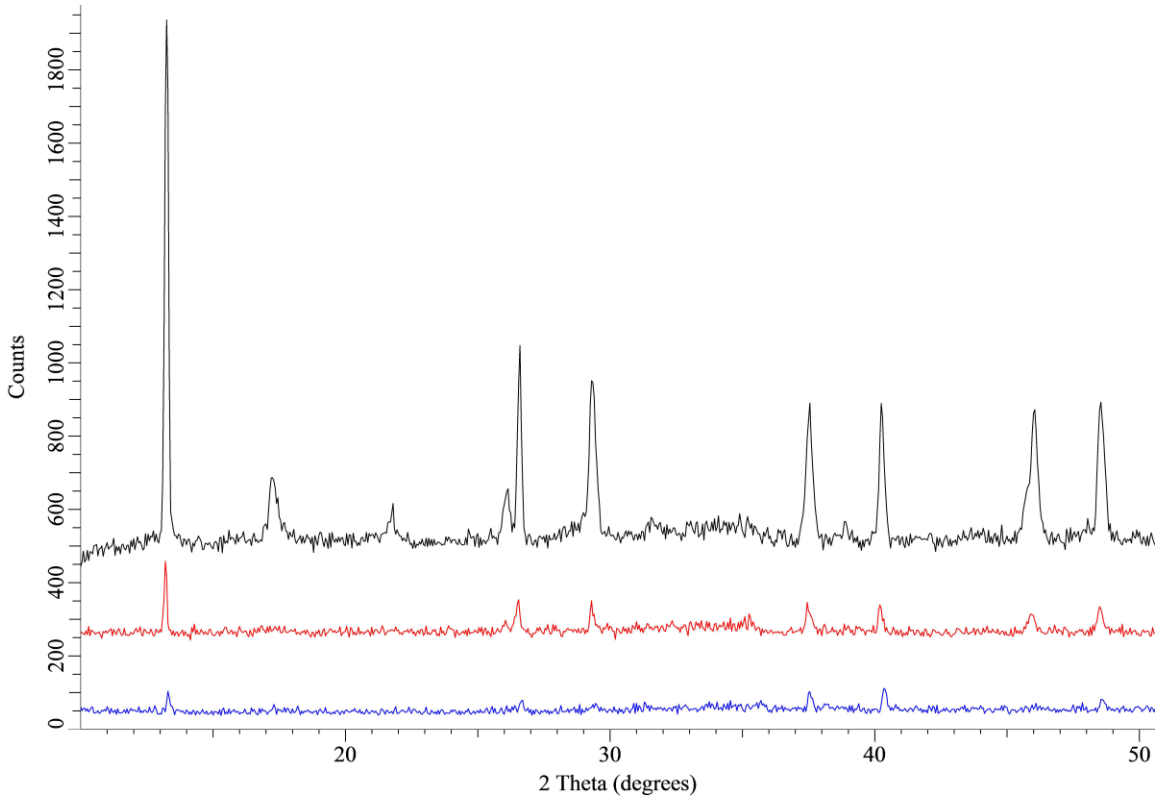

Figure 4. Powder X-ray diffraction patterns for Na_xLiCoS_2 ($0 \leq x \leq 1$). $NaLiCoS_2$ (black), oxidized $Na_{0.4}LiCoS_2$ (red) from the reaction of $NaLiCoS_2$ and a 0.6 mole fraction of iodine, Na_xLiCoS_2 ($x < 0.1$) (dark blue) from the reaction of $NaLiCoS_2$ and a stoichiometric excess of oxidant.

Frustration with the instability of $NaLiCoS_2$ led us to search for a more stable, well-behaved layered material for study. With the recent interest in MoS_2 and related layered sulfides, and our experience in studying air-sensitive compounds, $LiVS_2$ was decided upon for further investigation. Our initial probing of chemically oxidized samples gave unexpected results, with previously unobserved peaks appearing at low angles in measured diffraction patterns. These new observed phases of $LiVS_2$ had not been previously reported, which warranted further study.

Electrochemical Characterization of $LiVS_2$.

The electrochemical oxidation of $LiVS_2$ is straightforward, generating 1 mole of electrons per mole of VS_2 generated:

$$LiVS_2 \rightarrow Li^+ + VS_2 + e^-$$

This reaction proceeds by accessing the V^{3+}/V^{4+} redox couple, along with the diffusion of lithium ions out of the interlayer gallery. The primary electrochemical methods used to characterize $LiVS_2$ were chronopotentiometry and cyclic voltammetry.

As-synthesized Li_xVS_2 was analyzed by cyclic voltammetry to measure reversible redox behavior over multiple cycles. A typical cyclic voltammogram of Li_xVS_2 is presented in Figure 5. In this example the first cycle begins at the measured open circuit potential of the cell and is brought up to 3.5 V. For each subsequent cycle the potential is swept from 3.5 V to 1.75 V at a rate of typically 1 mV/s. Early reduction cycles show two peaks below 2.5 V which gradually merge as the cell is conditioned. Typically very uniform redox curves were observed between five and twenty cycles.

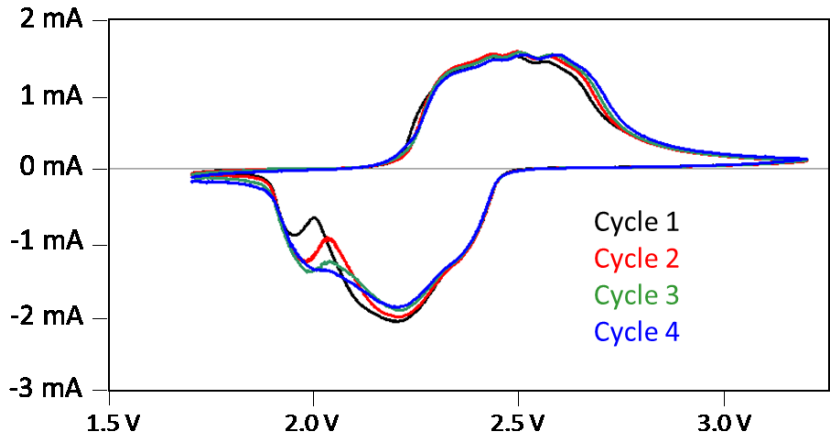

Figure 5. Typical cyclic voltammogram of $LiVS_2$. Reversible redox activity observed between 1.75 V - 3.5 V.

$LiVS_2$ was also analyzed by chronopotentiometry with an initial reduction to 1.0 V vs. lithium, followed by a continuous oxidation to a potential of 3.8 to 4.0 V. Experimental oxidation and reduction rates were calculated coulombically such that for a given electrochemical cell, the $LiVS_2$ content would be fully oxidized to VS_2 over a period of 24 hours. Previous studies[19] along with our own analysis has shown as-synthesized $LiVS_2$ to be lithium deficient. Investigating stoichiometric $LiVS_2$ necessitates an initial reduction, typically by exposure to an organolithium compound or by electrochemical reduction in a Li/Li^+ environment.

In a typical experiment, the electrode mixture was prepared using 10-20 mg of active material, with the masses of graphite and PVDF scaled to the desired 70:20:10 ratio. For example, a given electrochemical cell might contain 18.6 mg of Li_xVS_2, equal to 152 μmol assuming a fully reduced mass of 122.0125 g/mol. By conversion using Faraday's constant, a 152 μmol sample will require the exchange of 14.7 C total charge for the complete oxidation to VS_2. This total charge can then be converted to electrochemical current, as 1C = 1A · 1sec. For this example a current of 170 μA would be delivered over a 24 hour period. The overall calculation for the oxidation/reduction current can be summarized as:

$$\text{Current (A)} = \#\text{ mol } LiVS_2 \times 96458\ \text{C}\cdot\text{mol}^{-1} \times 1\ \text{A}\cdot\text{sec}\cdot\text{C}^{-1} \div 86400\ \text{sec.}$$

These experiments were used to estimate the oxidation state of as-synthesized $LiVS_2$, as well as explore any possible phase changes that were known to occur during oxidation. Figure 6 contains data from a typical reduction chronopotentiometry experiment. The 'plateau' regions observed during chronopotentiometry correspond to

reversible changes in the stoichiometry of Li_xVS_2. Under a fixed reducing current, the potential remains relatively constant before a sharp inflection is observed.

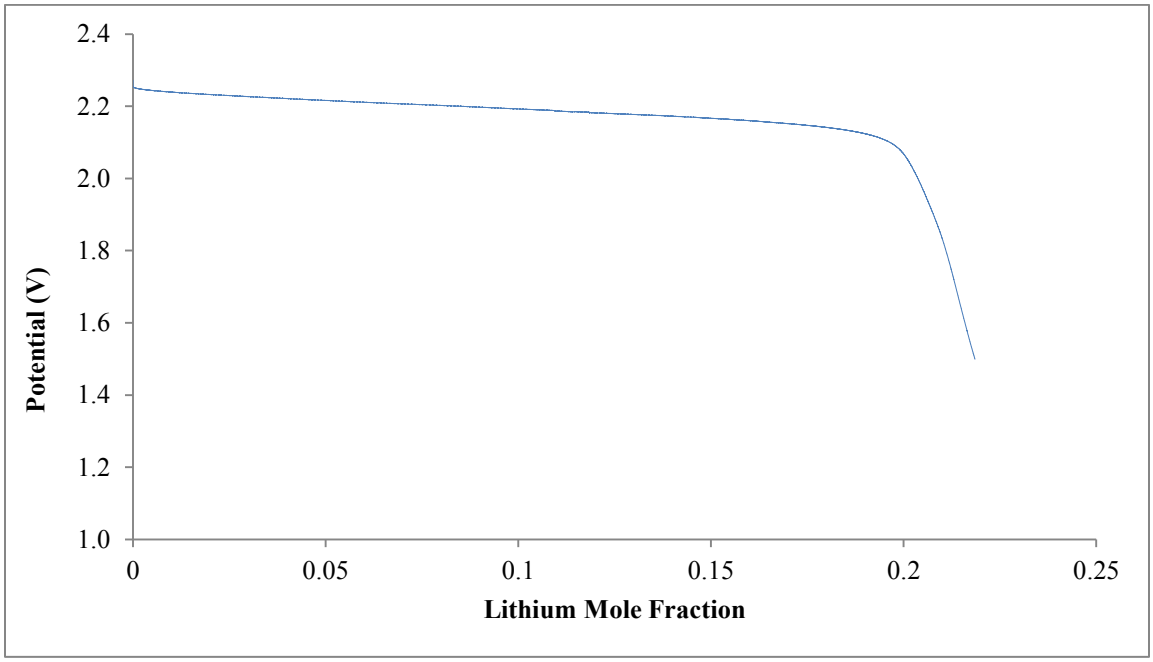

Figure 6. Typical reduction chronopotentiometry of as-synthesized Li_xVS_2. X-axis expressed as additional lithium mole fraction intercalated, calculated from reduction current and duration.

Following the reduction to $LiVS_2$ an oxidizing current of equal magnitude is applied while the potential is measured. A typical oxidation chronopotentiometry curve of $LiVS_2$ is presented in Figure 7. The reduction and oxidation plateaus of corresponding plots can be used to estimate the lithium deficiency of the as-synthesized Li_xVS_2.

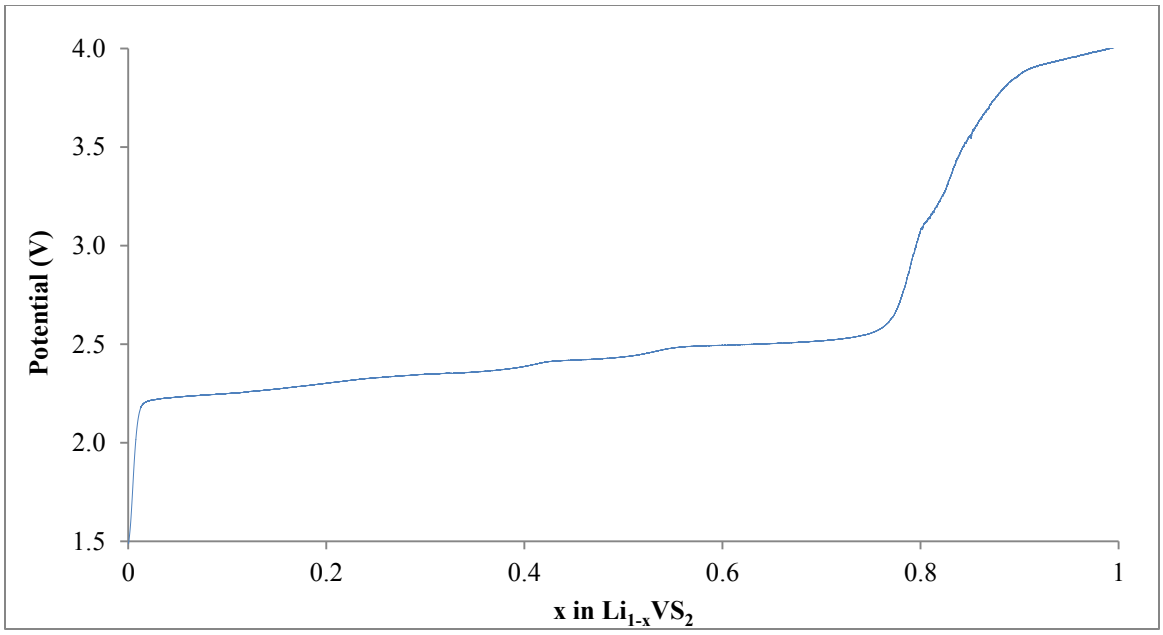

Figure 7. Typical chronopotentiometric oxidation of previously reduced $LiVS_2$. X-axis expressed as mole fraction of lithium removed during oxidative deintercalation.

During the initial reduction the active Li_xVS_2 is fully lithiated (x=1) upon which a sharp inflection in applied voltage occurs. Reductions are limited to 1.5 V vs. lithium anode to prevent access of the $LiVS_2/Li_2VS_s$ redox couple.[20] As the reduction/oxidation curves for a given experiment are generated using identical current densities, a ratio of the plateau durations can be used to estimate the lithium ion content of the starting material. For example, the original formula for a sample of Li_xVS_2 requiring approximately 17 ks to reach the inflection during reduction and approximately 68 ks during oxidation can be estimated as $Li_{0.75}VS_2$. Using this method we have determined the lithium contents of as-synthesized $LiVS_2$ to vary between 0.75 – 0.8 Li by formula weight.

The oxidation plateau also contains several minor inflections at approx. 0.5 and 0.33 Li ion content, which correspond to the 'α' and 'β' phases that have been described

previously as hexagonal, apparently monoclinic distorted lattices of the parent 1T-$LiVS_2$ '3s' phase.[21] Figure 8 illustrates the relationship between these phases, where at room temperature the $LiVS_2$ phase is stable when oxidized to about $Li_{0.8}VS_s$, where the β phase appears. Further oxidation generates a secondary α phase in Li_xVS_2, with complete oxidation yielding the fully delithiated VS_2.

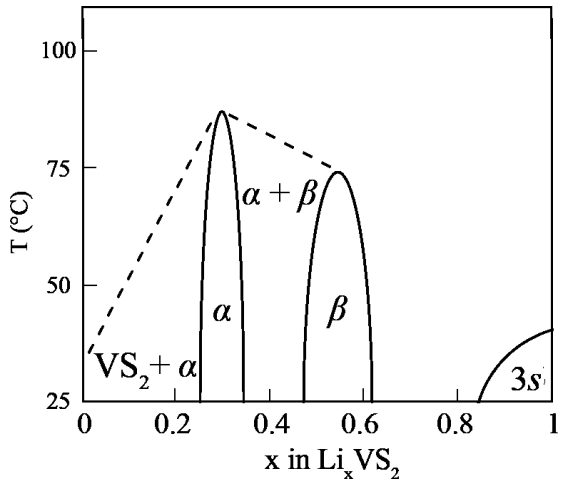

Figure 8. Partial phase diagram of Li_xVS_2 for lithium mole fractions 0 to 1. Temperature dependence is not relevant to the present work, as all measurements were taken at room temperature. Originally from Murphy, D. W., *et al*.[19]

These intermediate phases are distorted unit cells brought about by volume changes and altered coordination environments within the crystalline structure as oxidation occurs. Figure 8 illustrates how a solid solution exists for the individual 3s, β, and α phases where x may vary over a specific range in Li_xVS_2. From the diagram, it can be expected that one or more phases may coexist depending on oxidation extent and reaction conditions. During oxidation, the three phases (α, β, VS_2) can often be observed together by X-ray diffraction.

Solvation of Oxidized Li_xVS_2.

A series of Li_xVS_2 samples were prepared by chemical oxidation as previously described, with stoichiometric lithium contents of 0.8, 0.6, and 0.5-0.0. Acetonitrile was used as a solvent in these reactions, owing to its ease of removal by evaporation and being the favored solvent for this type reaction. Due to the layered nature of $LiVS_2$, diffusion of cations or overall perturbation of the interlayer gallery should induce observable changes in the interlayer spacing, which can be evidenced by careful examination of measured X-ray diffraction patterns. The reaction between iodine and $LiVS_2$ is a straightforward two electron process, with 1 mole of iodine capable of completely oxidizing 2 moles $LiVS_2$:

$$\tfrac{1}{2}\ I_2 + LiVS_2 \rightarrow LiI + VS_2$$

By combining these reactants in the aforementioned stoichiometric ratios, sufficient quantities of oxidized Li_xVS_2 samples were prepared for further solvation study. An additional VS_2 sample was prepared using a stoichiometric excess of iodine, as the stoichiometric VS_2 samples showed signs of incomplete reaction evidenced by XRD patterns of the oxidized Li_xVS_2 series.

Figure 9 contains X-ray patterns for as-prepared Li_xVS_2 saturated with acetonitrile, where x is the fraction of interlayer lithium cations present in the host compound, which can be expressed as the relative extent of oxidation. Small amounts of each oxidized fraction (5-10 mg) were used for each measurement. Saturated measurements were achieved by ensuring that the samples were dampened with clean solvent (CH_3CN in this case) and sealed with polyamide tape to prevent evaporation prior

to X-ray measurement. It was observed that successive oxidation leads to a decrease in relative intensity of the primary $LiVS_2$ peak at 14.4° 2θ and a "shoulder" peak, which appears at 14.5° 2θ and shifts to 14.7° 2θ as $x \rightarrow 1$. The formation of VS_2 is observed as the appearance of a peak at 15.4° 2θ, which is most significant at lithium mole fractions < 0.2.

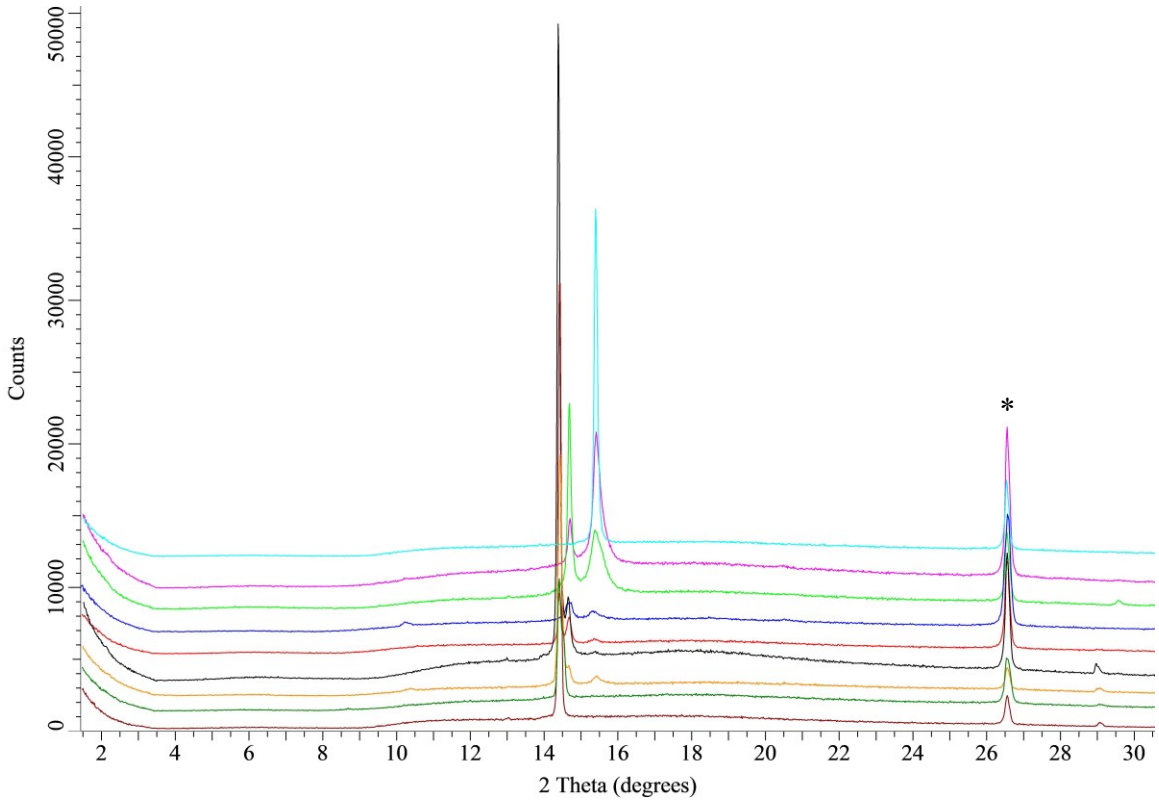

Figure 9. Stacked X-ray diffraction patterns of Li_xVS_2 exposed to acetonitrile. Ordered by decreasing cation density from bottom: $LiVS_2$ (burgundy), $Li_{0.8}VS_2$ (dark green), $Li_{0.6}VS_2$ (yellow), $Li_{0.4}VS_2$ (black), $Li_{0.3}VS_2$ (red), $Li_{0.2}VS_2$ (dark blue), $Li_{0.1}VS_2$ (bright green), VS_2 prepared from stoichiometric oxidation (magenta), VS_2 prepared from excess oxidant (light blue). Graphite denoted by asterisk (*).

No significant peaks are observed below 10° 2θ in any of the oxidized samples when exposed to acetonitrile. X-ray patterns are stacked vertically according to oxidation extent, beginning with the primary peak at 14.4° 2θ for reduced $LiVS_2$ (shown in burgundy), followed by samples with approximately 80%, 60%, and 40 - 0% (by 10%

intervals) lithium content remaining. Successively oxidized samples show a general trend towards disappearance of $LiVS_2$ with the growth of a second Li_xVS_2 phase and eventual complete conversion to VS_2.

The measured peaks present at 26.5° 2θ are due to graphite, which was included in samples as a standard for calibration. Each sample was prepared by depositing small amounts of powder on top of a flat zero background plate, and slight variations in sample height are unavoidable. These variations will induce a shift in the measured XRD pattern, necessitating the additional graphite standard for relative comparisons. Patterns were stacked and shifted where necessary to align the measured graphite peaks. It should be noted that the specific instrument used attenuates the measured pattern below 10° 2θ, while the upturn in signal below 3° 2θ is due to stray un-diffracted X-rays reaching the detector.

Figure 10 gives an expanded view of X-ray patterns for as-prepared Li_xVS_2 saturated with acetonitrile. The appearance of a higher angle "shoulder" in the primary peak at 14.4° 2θ (**1**) is clearly visible in the $Li_{0.8}VS_2$ pattern. This additional peak is centered at 14.5° 2θ (**2**) and appears to shift slightly higher in angle to 14.7° 2θ relative to the oxidation extent of Li_xVS_2. Further oxidation leads to the growth of a peak centered at 15.4° 2θ (**3**) corresponding to the VS_2 phase. Peak **2** is evidence of a metastable lithium deficient phase with a reduced interlayer distance. Visually, the disappearance of **1** is coincident with the growth of **2**, which in turn leads to disappearance of **2** and growth of **3**. In the oxidation range of 20 - 70%, or for Li_xVS_2 (where $0.3 > x > 0.8$), two $LiVS_2$ phases are present in varying ratios.

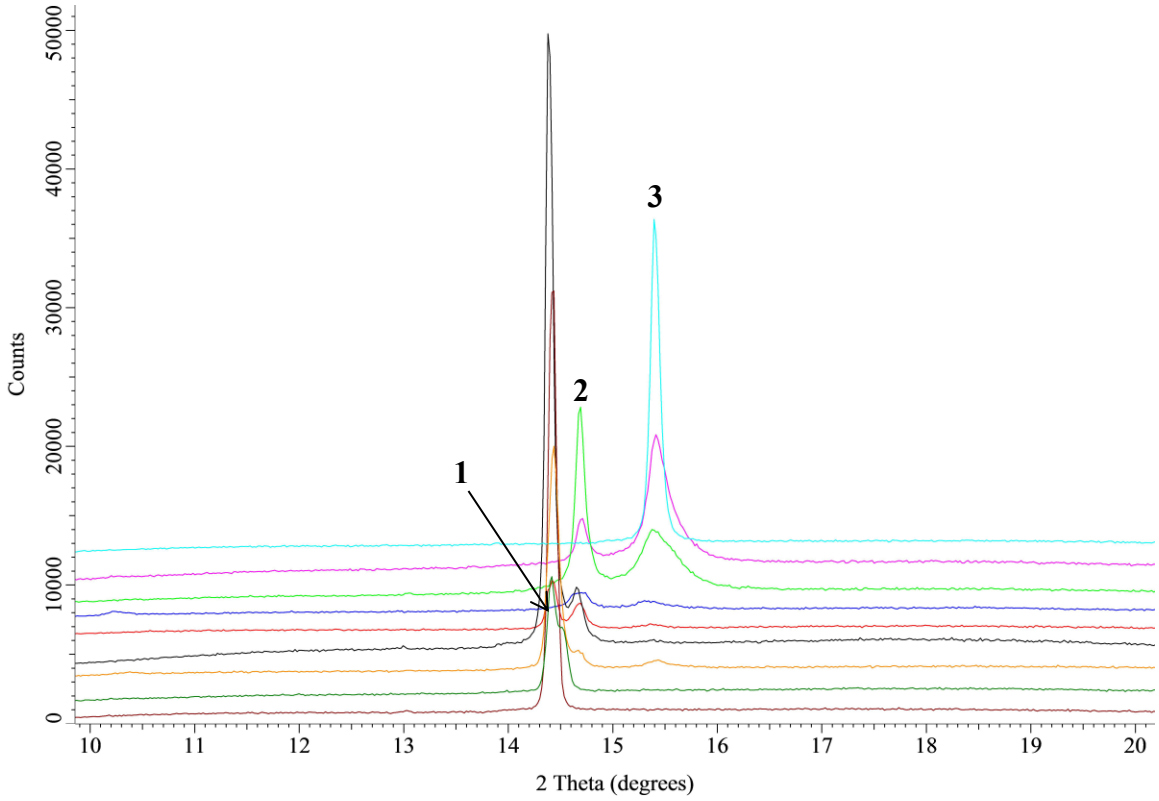

Figure 10. Expanded view of Li_xVS_2 exposed to acetonitrile. $LiVS_2$ (burgundy), $Li_{0.8}VS_2$ (dark green), $Li_{0.6}VS_2$ (yellow), $Li_{0.4}VS_2$ (black), $Li_{0.3}VS_2$ (red), $Li_{0.2}VS_2$ (dark blue), $Li_{0.1}VS_2$ (bright green), VS_2 prepared from stoichiometric oxidation (magenta), VS_2 prepared from excess oxidant (light blue).

It is reasonable to assume that bulk solvation of Li_xVS_2 by acetonitrile would present as a lower angle peak in the diffraction pattern. A qualitative assessment of Figure 9 suggests there is no significant presence of acetonitrile solvated Li_xVS_2 phases present over the range oxidation extents tested. It may be possible that small inclusions of acetonitrile occur at the edges or defect sites of Li_xVS_2 crystallites; however any long-range ordered expansion of the interlayer distance would produce a measurable signal in the XRD pattern.

V. SOLVATION OF Li_xVS_2 BY N-METHYL AMIDES

Additional tests were performed on the fractionally oxidized Li_xVS_2 samples previously synthesized, in order to examine the intercalation of different solvents into the interlayer gallery. Small Li_xVS_2 portions were dried under argon then saturated with one of the N-methyl formamides (where N = 0, 1, or 2, corresponding to formamide, N-methylformamide, and N,N-dimethylformamide, respectively) and analyzed by XRD for signs of solvated phases. The XRD patterns for these measurements were compared to the oxidized series exposed to acetonitrile. As the samples were prepared and handled in an identical manner, any measured differences should be attributable to phase changes brought about by solvation or further reaction with the solvent species alone.

Figures 11 presents XRD patterns for the oxidized Li_xVS_2 series after exposure to formamide. In contrast to what was observed in fractionally oxidized samples exposed to acetonitrile, evidence of new solvated phases is observed in these samples after oxidation. A noticeable difference is seen in the first oxidized sample $Li_{0.8}VS_2$, where a shoulder peak at 14.5° 2θ was initially observed in the presence of acetonitrile but is absent in the presence of formamide. Further oxidation leads to the appearance of several new peaks, presented in Table 1. As in the acetonitrile series, the primary $LiVS_2$ peak at 14.4° 2θ is present in all oxidized samples down to $Li_{0.3}VS_2$, after which it is not observed. The fully reduced $LiVS_2$ shows no sign of reaction after being exposed to formamide.

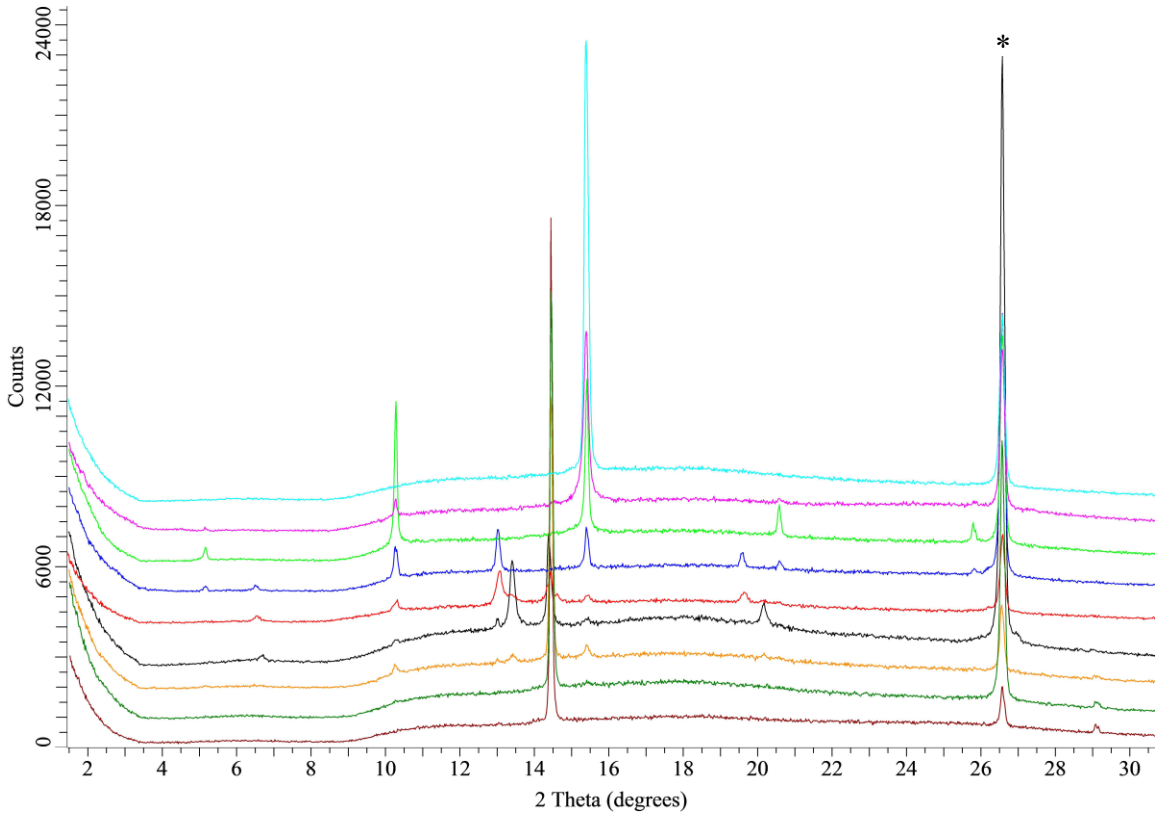

Figure 11. Stacked X-ray diffraction patterns of Li_xVS_2 exposed to formamide. Ordered by decreasing cation density from bottom: $LiVS_2$ (burgundy), $Li_{0.8}VS_2$ (dark green), $Li_{0.6}VS_2$ (yellow), $Li_{0.4}VS_2$ (black), $Li_{0.3}VS_2$ (red), $Li_{0.2}VS_2$ (dark blue), $Li_{0.1}VS_2$ (bright green), VS_2 prepared from stoichiometric oxidation (magenta), VS_2 prepared from excess oxidant (light blue). Graphite denoted by asterisk (*).

When comparing the X-ray patterns for acetonitrile and formamide, there is clearly a more complicated interaction occurring between Li_xVS_2 and formamide. As none of these new peaks were observed in the same oxidized samples with acetonitrile, their presence is indication of one or more formamide-solvated Li_xVS_2 phases. The first low intensity peak observed at 10.3° 2θ in $Li_{0.6}VS_2$ is likely a second order reflection of the peak observed in $Li_{0.3}VS_2$ and $Li_{0.2}VS_2$ at 5.15° 2θ. The reasoning for this is twofold; the d-spacing of the higher angle peak is exactly twice that of the lower peak, and the relative intensities of both peaks seem to be related at higher oxidation states. Additionally from the primary peak location, any third order reflections would be present

at 15.45° 2θ, which would overlap the peak from VS_2 at 15.4° 2θ. These three peaks are indication of a formamide-solvated Li_xVS_2 phase with an interlayer spacing of approximately 17.1 Å. This represents an interlayer expansion of about 11 Å from the fully reduced $LiVS_2$ phase.

Table 1. Solvation peaks observed in Li_xVS_2 samples exposed to formamide. *Mole fraction corresponding toVS_2 prepared with stoichiometric excess of oxidant.

Angle (2θ)	Apparent d-spacing (Å)	Lithium Mole Fraction
5.2°	17.0	0.2 - 0.1
6.5°	13.6	0.4 - 0.2
10.3°	8.6	0.6 - 0.1
13.0°	6.8	0.6 - 0.2
13.4°	6.6	0.6 - 0.3
15.4°	5.7	0.6 - 0.0*

At intermediate oxidation states of Li_xVS_2 (x = 0.2, 0.3, 0.4) the peak observed at 6.5° 2θ and its second order reflection at 13.0° 2θ are evidence of a second formamide solvated Li_xVS_2 phase, with an interlayer spacing of approximately 13.6 Å. The intensities of the concurrent peaks observed at 13.0° and 13.4° 2θ appear to be inversely related. This may indicate two closely related Li_xVS_2 phases, having an interlayer spacing difference of only 0.1 Å with subtle differences in the interlayer solvent packing arrangement, which shifts towards a larger interlayer spacing as oxidation proceeds.

Figure 12 contains x-ray diffraction patterns of the oxidized Li_xVS_2 series exposed to N-methylformamide. A new peak is present at 6.3° 2θ after oxidation to $Li_{0.6}VS2$, with a second order reflection peak centered at 12.6° 2θ. Additionally, a new peak is present at 14.6° 2θ in $LixVS_2$ ($0.3 < x < 0.1$) possibly due to the same Li-deficient

phase observed in the acetonitrile series. These new peaks indicate a single N-methylformamide solvated Li_xVS_2 phase is present when $0.6 < x < 0$, with an apparently un-solvated β or α phase present at higher oxidation states. The average interlayer distance of this new phase is approximately 14 Å, calculated from the peak position of 6.3° 2θ.

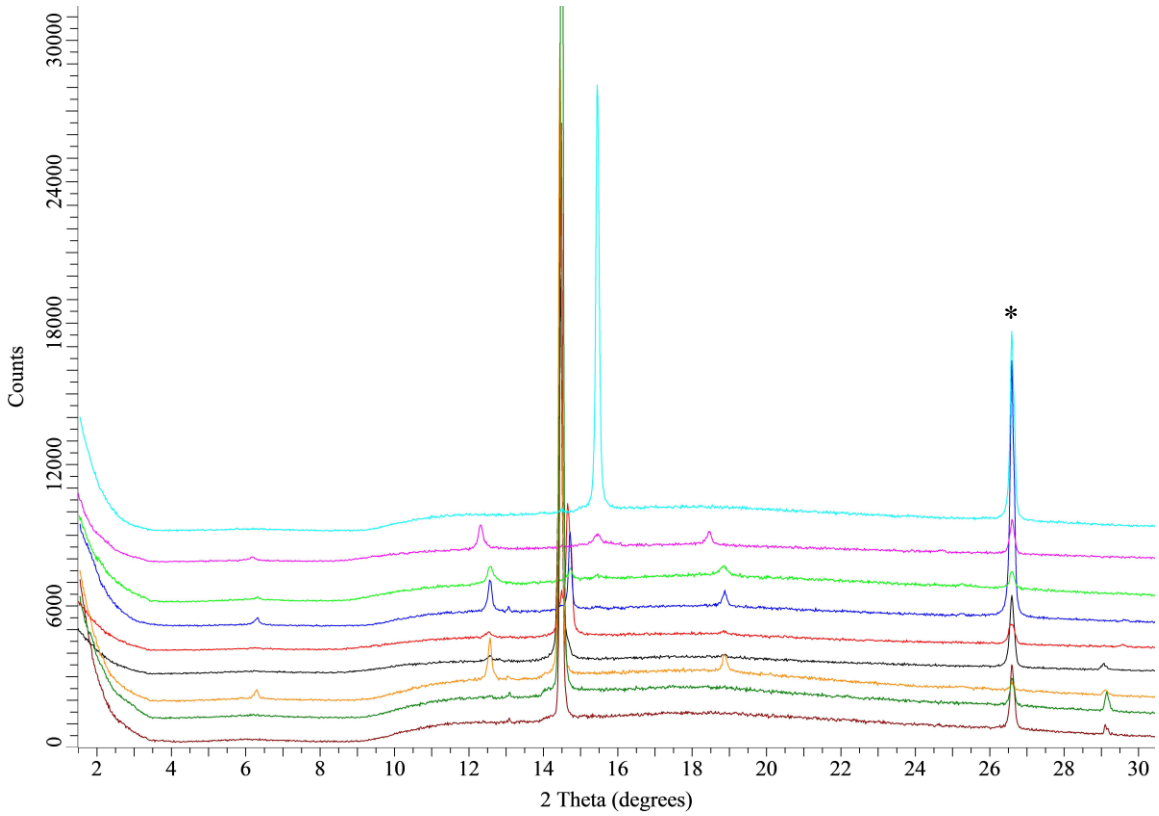

Figure 12. Stacked X-ray diffraction patterns of Li_xVS_2 exposed to N-methylformamide. Ordered by decreasing cation density from bottom: $LiVS_2$ (burgundy), $Li_{0.8}VS_2$ (dark green), $Li_{0.6}VS_2$ (yellow), $Li_{0.4}VS_2$ (black), $Li_{0.3}VS_2$ (red), $Li_{0.2}VS_2$ (dark blue), $Li_{0.1}VS_2$ (bright green), VS_2 prepared from stoichiometric oxidation (magenta), VS_2 prepared from excess oxidant (light blue). Graphite denoted by asterisk (*).

X-ray diffraction patterns of the oxidized Li_xVS_2 series exposed to N,N-dimethylformamide (DMF) are presented in Figure 13. Several peaks are observed after partial oxidation at 5.35°, 10.7°, and 16.0° 2θ. These appear to be due to the same phase, with the two higher angle peaks being second and third order reflections of the low

angle peak at 5.35° 2θ, with a corresponding d-spacing of 16.5 Å. The solvation peaks in DMF are comparatively higher in intensity compared to those observed in formamide and N-methylformamide. The reason for this relative difference in intensity cannot be directly quantified with the data presented. It is possible that intercalated DMF molecules adopt a more highly ordered interlayer packing arrangement, which could directly correlate to higher measured peak intensities.

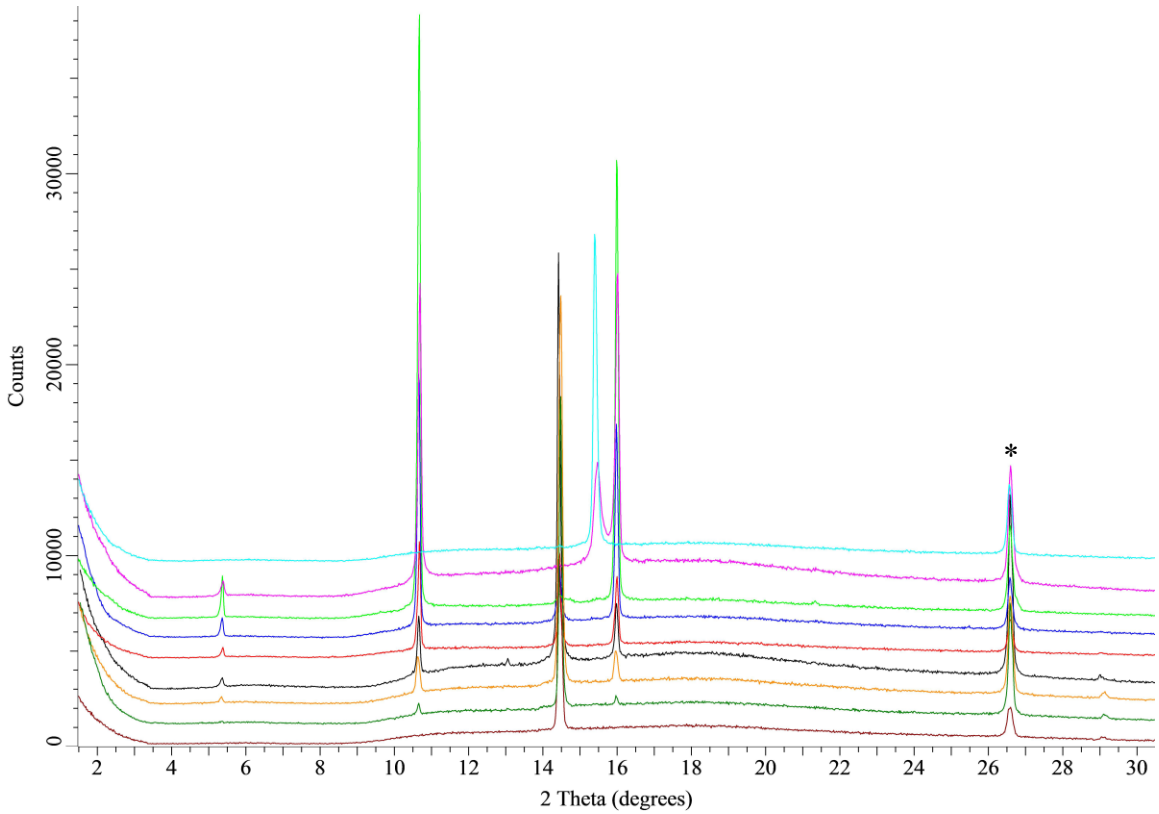

Figure 13. Stacked X-ray diffraction patterns of Li_xVS_2 exposed to N,N-dimethylformamide. Ordered by decreasing cation density from bottom: $LiVS_2$ (burgundy), $Li_{0.8}VS_2$ (dark green), $Li_{0.6}VS_2$ (yellow), $Li_{0.4}VS_2$ (black), $Li_{0.3}VS_2$ (red), $Li_{0.2}VS_2$ (dark blue), $Li_{0.1}VS_2$ (bright green), VS_2 prepared from stoichiometric oxidation (magenta), VS_2 prepared from excess oxidant (light blue). Graphite denoted by asterisk (*).

Comparison of the X-ray diffraction patterns of Li_xVS_2 exposed to N-methyl formamides reveals several common trends. Stoichiometric $LiVS_2$ does not appear to react with the N-methyl formamides, as the XRD patterns for these samples and as-

synthesized $LiVS_2$ are identical. Curiously, the stoichiometrically oxidized VS_2 samples (magenta) exhibit signs of intercalation, whereas VS_2 samples prepared by a stoichiometric excess of oxidant (light blue) show only the single VS_2 phase by XRD. This is likely due to incomplete oxidation of $LiVS_2$ through side reactions with impurity phases left over during synthesis.

Intermediate oxidation extents of Li_xVS_2 ($x < 1$) show clear evidence for intercalated phases when exposed to N-methyl formamides. From the acetonitrile series, a general transition between phases is observed in Li_xVS_2 where the 3s phase (from Figure 9) is converted to the β and α phases beginning at x=0.6. None of the 3s phase is observed in XRD patterns after oxidation to $Li_{0.2}VS_2$, while the remaining phase(s) are a mixture of the distorted phases. These trends are mirrored in the N-methylformamide series, where solvated phases are observed only after a phase change occurs from some degree of oxidation. Both the formamide and N-methylformamide series show signs of a solvated phase after oxidation to $Li_{0.6}VS_2$, with the DMF series beginning to solvate at $Li_{0.8}VS_2$. Also in both the formamide and N-methylformamide series the 3s phase is no longer observed after oxidation to $Li_{0.2}VS_2$.

The layered structure of $LiVS_2$ dictates that intercalation of guest molecules will occur at the exposed edges of crystallites. The extent of inclusion of these guest molecules is likely dependent on the interlayer environment, where increased layer spacing and a reduction in cation density should promote intercalation. The observation that stoichiometric $LiVS_2$ does not form solvated phases in the presence of N-methyl formamides is likely due to high cation density and interlayer attraction. Also the VS_2 samples prepared from a stoichiometric excess of oxidant show no indication of solvation

by N-methyl formamides, which are apparently excluded from the interlayer gallery by the Van der Waals interaction between layers.

Two distinct phases are observed in the oxidized Li_xVS_2 series exposed to formamide, with approximate interlayer spacings of 13.6 Å and 17.1 Å which constitute an increase of 7.5 Å and 11.0 Å respectively from native $LiVS_2$. The theoretical minimum length of a formamide molecule is about 2.6 Å, calculated from average bond lengths and angles of the constituent atoms. Without single-crystal data of these intercalated phases, it is difficult to determine the interlayer packing arrangement of the solvent species. However from the increase in layer spacing of 7.5 Å, it is likely the first solvated phase is due to a double layer of formamide molecules sharing the interlayer volume while coordinating to remaining lithium cations. The spacing of second formamide-solvated phase is only 3.5 Å more than the first, which may indicate an expanded packing arrangement, or effects caused by solvent-solvent interactions.

A single solvated phase is observed in the oxidized Li_xVS_2 series exposed to methyl formamide, with an interlayer spacing of approximately 14 Å. This distance is slightly larger than that measured for the first formamide solvated phase. This is not a surprising result, with additional methyl group making this solvent molecule physically larger than formamide, an interlayer packing arrangement would likely require more volume.

In the DMF series the 3s phase (typically associated with Li_xVS_2, $0.8<x<1$) was observed even in $Li_{0.2}VS_2$ while not being present in a similarly oxidized sample in acetonitrile. This is interesting as the same oxidized sample was used to prepare both samples, a portion of the acetonitrile was simply evaporated from a $Li_{0.2}VS_2$ sample prior to DMF solvation. The reappearance of the 3s phase in $Li_{0.2}VS_2$ must be due to an interaction with the DMF solvent. One possible explanation for this behavior is that DMF is more strongly coordinating and is able to displace the lithium ions for optimal solvation, generating the 3s phase as a byproduct where the lithium ions are more concentrated.

This may allow DMF to act as a 'solvent wedge' (Figure 14) able to intercalate Li_xVS_2 by establishing a local (low) concentration of mobile lithium cations appropriate for solvation even if the *average* ion concentration in the sample is too high. In acetonitrile alone, $LiVS_2$ transitions to the distorted β and α phases after removal of sufficient lithium cations. However if Li_xVS_2 crystallites were intercalated by a strongly coordinating species this would drive lithium ions inward, allowing preservation of the 3s phase in the particle interior, and establishing an appropriately low cation concentration in the exterior to allow for solvation. Li_xVS_2 begins to solvate at higher lithium content in the presence of DMF, and only generates a single solvated phase. This phase appears highly crystalline, based on relative signal intensity observed in powder XRD patterns.

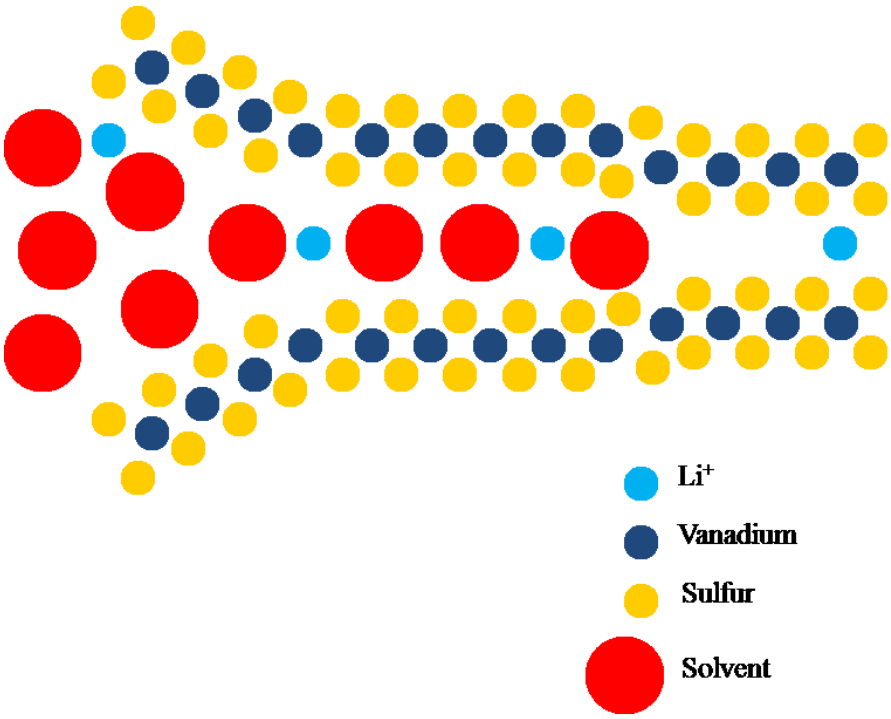

Figure 14. Representation of 'solvent wedge' intercalation process. A strongly coordinating Lewis base may be able to overcome interlayer Van der Waals attraction and solvate remaining interlayer cations.

The differences observed in solvating character of the N-methyl formamides are likely due to the relative size of the solvent molecules. The measured interlayer spacing of intercalated phases increases with increasing guest molecule size, where the Van der Waals radii of $C_3H_7NO > C_2H_5NO > CH_3NO$. The specific orientation of the intercalated molecules cannot be determined by power XRD data alone; however assumptions can be made about the interlayer packing arrangement. The carbonyl moiety of these solvents is expected to act as a Lewis base and coordinate with interlayer cations, while the cations themselves remain coordinated to the sulfur atoms. However other possibilities remain; amines have been found to readily dissolve polysulfides and may be able to coordinate directly with the interlayer sulfur planes.

VI. SOLVATION OF Li_xVS_2 BY ALIPHATIC PRIMARY AMINES

Fractionally oxidized Li_xVS_2 samples ($1 < x < 0$) were exposed to several aliphatic amines. Hexylamine and aminodecane are both liquid a room temperature, and differ suitably in size. Additionally Jeffamine EDR-148, a commercially available polyetheramine with the linear formula $H_2N(CH_2CH_2O)_2CH_2NH_2$ was used in this study. Samples were prepared in a similar manner to the previously described for the N-methyl formamide series, being first dried and then saturated with an amine prior to analysis. X-ray diffraction patterns for each oxidized sample were measured and grouped by solvent species.

Figure 15 contains XRD patterns for the oxidized Li_xVS_2 samples exposed to hexylamine. Specifically in the pattern for $Li_{0.2}VS_2$, evidence of multiple solvated phases are observed as two small peaks located at 3.5° and 3.7° 2θ. Multiple order reflections of these peaks can be seen in the remaining patterns. Reflections of the peak at 3.5° 2θ do not appear to shift relative to oxidation extent, whereas neighboring reflections of the second peak at 3.7° 2θ show a general shift towards higher angle as oxidation of Li_xVS_2 proceeds. Evidence this second phase is also present in the stoichiometrically over-oxidized VS_2 samples with a peak present at 7.5° 2θ. From the peak angles of 3.5° and 3.7° 2θ, the interlayer distances of these two phases is approximately 25.2 Å and 23.8 Å respectively.

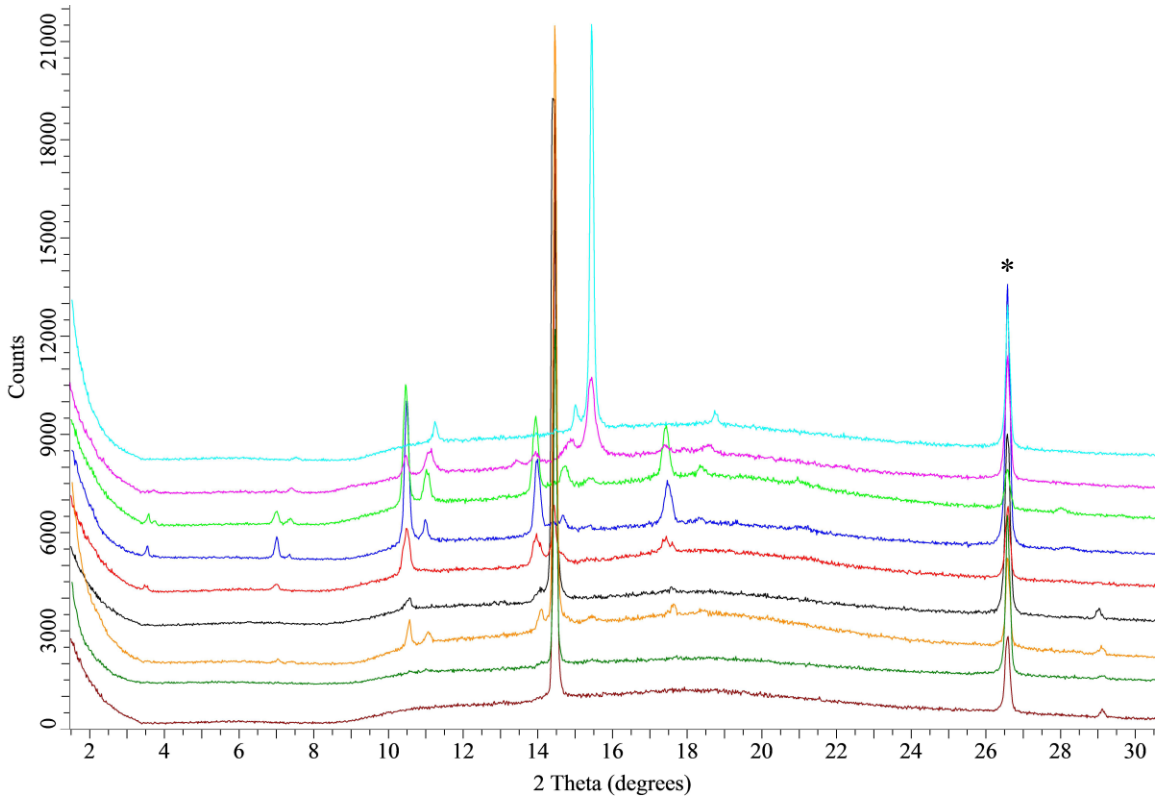

Figure 15. Stacked X-ray diffraction patterns of Li_xVS_2 exposed to hexylamine. Ordered by decreasing cation density from bottom: $LiVS_2$ (burgundy), $Li_{0.8}VS_2$ (dark green), $Li_{0.6}VS_2$ (yellow), $Li_{0.4}VS_2$ (black), $Li_{0.3}VS_2$ (red), $Li_{0.2}VS_2$ (dark blue), $Li_{0.1}VS_2$ (bright green), VS_2 prepared from stoichiometric oxidation (magenta), VS_2 prepared from excess oxidant (light blue). Graphite denoted by asterisk (*).

The measured expansion in interlayer spacing of these two phases is likely due to a bilayer packing arrangement of the intercalated hexylamine molecules, with the amine moiety directed towards VS_2 layers and the carbon tails forming an ordered paraffinic structure. The distance between carbon atoms in a linear hexylamine molecule is approximately 1.3 Å parallel to the carbon chain, calculated from the sp^3 C-C bond length of 1.54 Å and angle of 109.5°. A similar linear distance of 1.3 Å can be assumed between the C-N bonds, with an additional distance of 1.0 Å between the terminal N-H and C-H bonds. This gives a minimum approximate length of 10 Å for a linear hexylamine molecule, which is less than half the measured d-spacings of the hexylamine intercalated phases (23.8 Å and 25.2 Å). Intercalation of hexylamine is not observed to

occur in $LiVS_2$ or $Li_{0.8}VS_2$ which suggests the solvation is limited by cation density. The presence of two phases with similar interlayer spacing is curious, and may be due to the amine coordinating with either lithium cations or the layered sulfur planes. That the spacing of one phase remains constant while the other appears to shift relative to oxidation extent may be explained by the angle of the carbon tails of hexylamine. Figure 16 illustrates several possible packing arrangements of the intercalated solvent molecules. The *in situ* size of solvent molecules, coordination environment and molecular orientation are likely the major factors which determine packing. Ultimately without single crystal measurement of these phases it is difficult to assess the interlayer packing arrangement of guest species with any certainty.

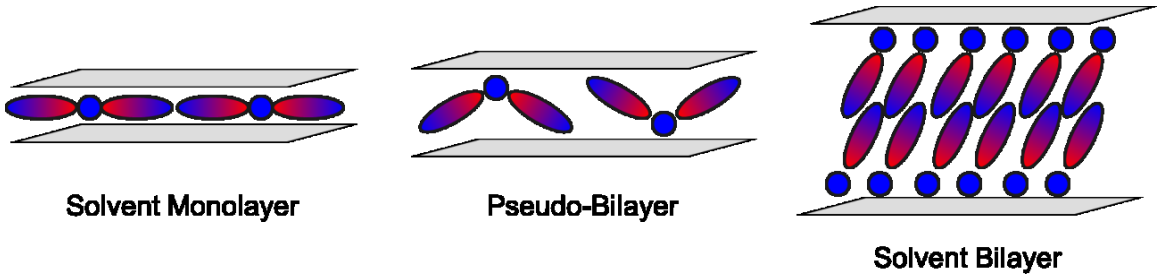

Figure 16. Diagram of proposed solvent packing arrangements between VS_2 layers. The Lewis base is assumed to coordinate directly to the remaining cations or possibly with the adjacent sulfur planes. Solvent molecules represented by shaded ellipsoids, lithium cations by solid blue circles.

Figure 17 contains XRD patterns of oxidized Li_xVS_2 exposed to aminodecane. The solvated peaks observed in $Li_{0.2}VS_2$ appear to be multiple order reflections of a single phase which is not observed due to signal attenuation by the instrument at low angles. The calculated d-spacings of these peaks are multiples of approximately 35.3 Å, indicating a single solvated phase is present during oxidation. The measured interlayer distance is again likely due to a bilayer forming from the intercalated aminodecane molecules, which may be adopting a paraffinic orientation where the carbon tails are

directed away from the Li_xVS_2 layer slabs. As before, a linear distance of 1.3 Å is assumed for C-C and C-N bonds and an additional 1.0 Å between N-H and C-H bonds in the aminodecane molecule, parallel to the carbon chain. This gives a minimum approximate length of 15 Å for a linear aminodecane molecule, roughly half the interlayer distance measured in the aminodecane-solvated phase.

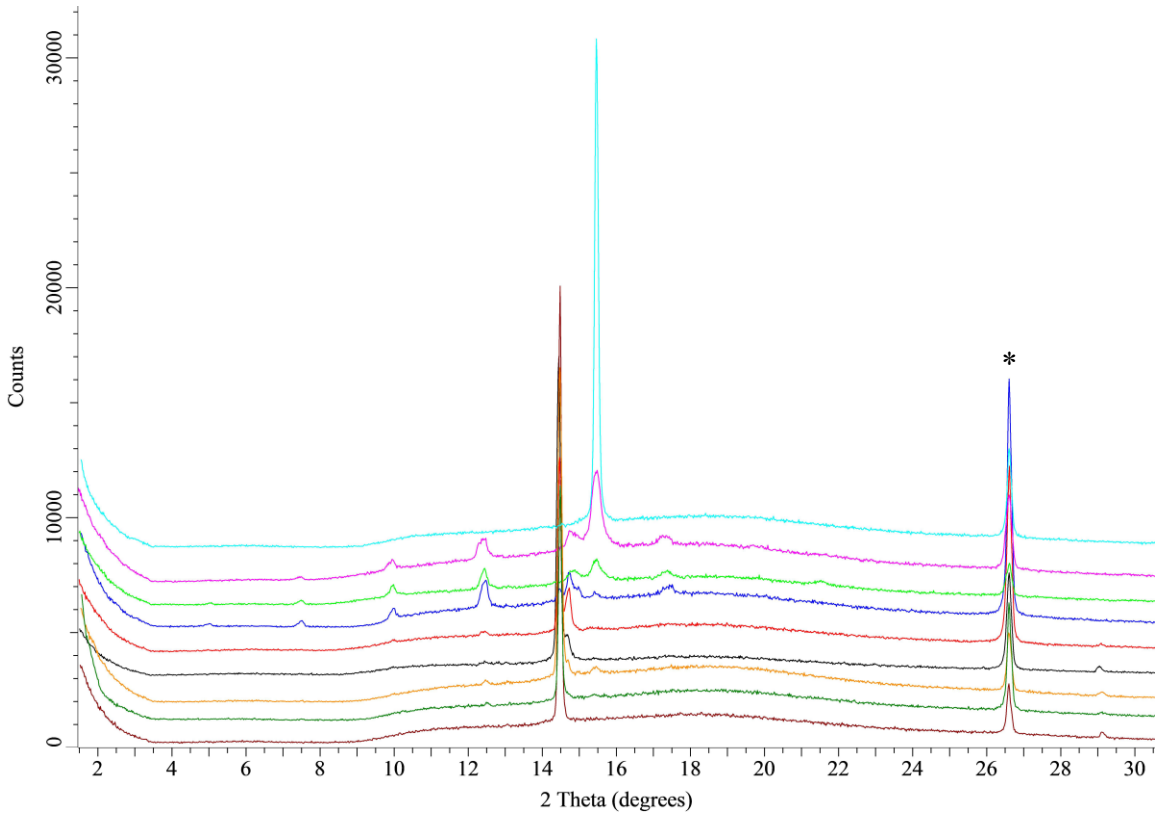

Figure 17. Stacked X-ray diffraction patterns of Li_xVS_2 exposed to aminodecane. Ordered by decreasing cation density from bottom: $LiVS_2$ (burgundy), $Li_{0.8}VS_2$ (dark green), $Li_{0.6}VS_2$ (yellow), $Li_{0.4}VS_2$ (black), $Li_{0.3}VS_2$ (red), $Li_{0.2}VS_2$ (dark blue), $Li_{0.1}VS_2$ (bright green), VS_2 prepared from stoichiometric oxidation (magenta), VS_2 prepared from excess oxidant (light blue). Graphite denoted by asterisk (*).

Previous measurements were taken of $Li_{0.4}VS_2$ solvated with aminodecane on a different instrument, as shown in Figure 18. The sample preparation was similar to the oxidized series presented herein; however the X-ray diffraction instrument used did not significantly attenuate low angle signals. Here the primary peak at ~2.5° 2θ is visible,

with remaining multiple order reflections at ~5.0°, ~7.5° 2θ, etc. Stoichiometric $LiVS_2$ does not appear to react with aminodecane, nor does the VS_2 prepared from a stoichiometric excess of oxidant.

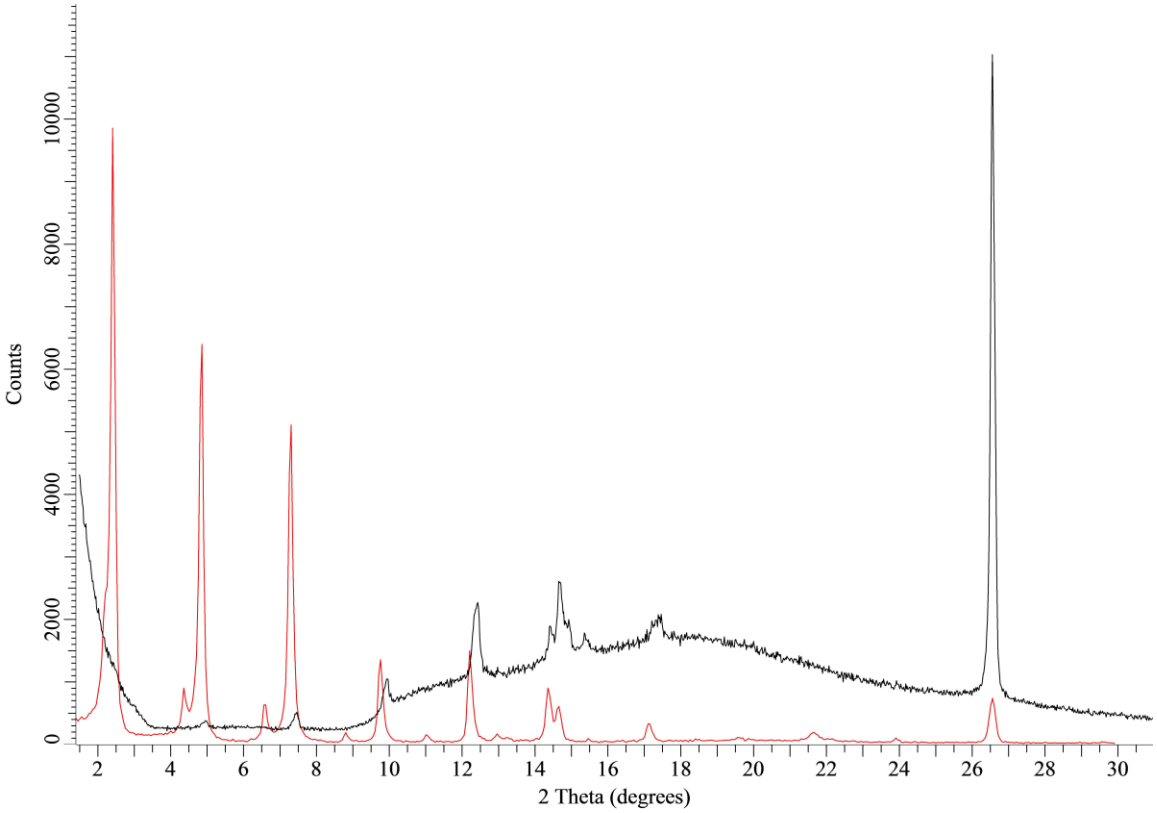

Figure 18. Comparison between powder X-ray diffractions patterns of aminodecane-solvated phases illustrating low-angle attenuation. XRD patterns of aminodecane-solvated $Li_{0.2}VS_2$ (black) measured on a Bruker D8 Advance, and aminodecane-solvated $Li_{0.4}VS_2$ (red) measured previously using a Bruker D8 Focus. Significant attenuation is obvious in first pattern, which is a consequence of the instrument design.

The final solvent used in this study is a polyetheramine known as Jeffamine EDR-148, which was included primarily due to its physical properties as a liquid amine at room temperature, and also due to its immediate availability. This compound has several commercial applications including use as a monomer in polyamide synthesis and as a plasticizing agent for thermoset polymers. Figure 19 contains XRD patterns for oxidized Li_xVS_2 samples exposed to this polyetheramine. The presence of solvated phases

evidenced by low angle peaks is consistent with many of the previous measurements. The low angle peaks observed in $Li_{0.2}VS_2$ indicate two separate solvated phases. The peak located at 6.6° 2θ and its second order reflection at 13.2° 2θ correspond to a layer spacing of 13.4 Å.

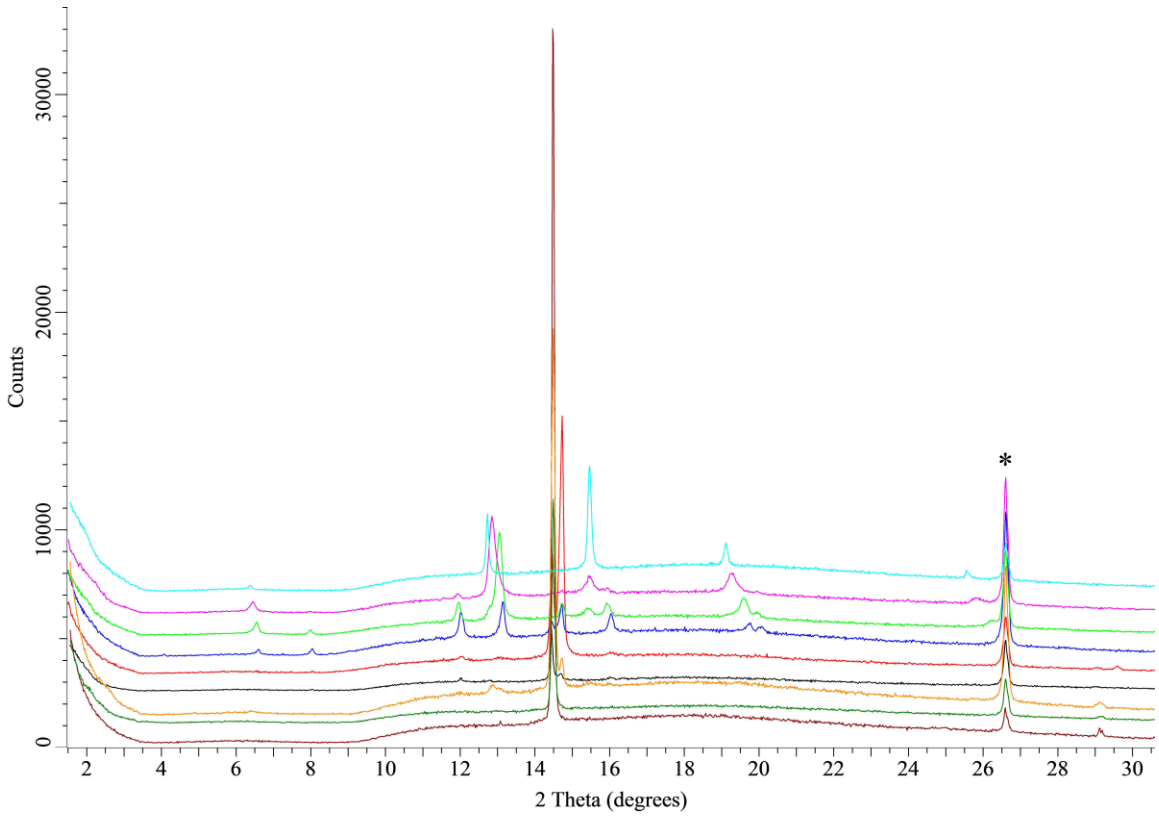

Figure 19. Stacked X-ray diffraction patterns of Li_xVS_2 exposed to the polyetheramine Jeffamine EDR-148. Ordered by decreasing cation density from bottom: $LiVS_2$ (burgundy), $Li_{0.8}VS_2$ (dark green), $Li_{0.6}VS_2$ (yellow), $Li_{0.4}VS_2$ (black), $Li_{0.3}VS_2$ (red), $Li_{0.2}VS_2$ (dark blue), $Li_{0.1}VS_2$ (bright green), VS_2 prepared from stoichiometric oxidation (magenta), VS_2 prepared from excess oxidant (light blue). Graphite denoted by asterisk (*).

The two additional low angle peaks at 8.0° and 12.0° 2θ are likely higher order reflections of an attenuated peak at 4.0° 2θ, which is not observed. This second phase would therefore have a d-spacing of approximately 22 Å, indicating this phase is due to a solvated bilayer. Consistent with previous observations, polyetheramine does not appear

to readily solvate stoichiometric $LiVS_2$, though solvated phases are observed in both stoichiometrically oxidized VS_2 and VS_2 prepared by a stoichiometric excess of oxidant.

A summary of interlayer spacings for the intercalated phases associated with different solvents tested here is presented in Table 2. In the majority of solvated phases, the measured interlayer distances are consistent with bilayer solvent packing arrangements. There is also an apparent relationship between the size of solvent molecules and the measured interlayer expansion.

Table 2. Summary of solvated phases observed in Li_xVS_2 and associated solvent species.

Solvent	Measured d-spacing of observed phase(s)	Interlayer expansion vs. LiVS2
Acetonitrile	No evidence of solvated phases observed	n/a
Formamide	Two solvated phases, 13.6 Å and 17.1 Å	7.5 Å, 11 Å
N-Methylformamide	One solvated phase, 14.0 Å	7.9 Å
N,N-Dimethylformamide	One solvated phase, 16.5 Å	10.4 Å
Hexylamine	Two solvated phases, 23.8 Å and 25.2 Å	17.7 Å, 19.1 Å
Aminodecane	One solvated phase, 35.3 Å	29.2 Å
Jeffamine EDR-148	Two solvated phases, 13.4 Å and 22.0 Å	7.3 Å, 15.9 Å

The data suggest that certain criteria must be met before rapid solvation of Li_xVS_2 can proceed. Solvation of Li_xVS_2 appears to be a diffusion limited process, and is expected to proceed at values of x below a threshold, given a suitably coordinating Lewis base and sufficient time. Previous studies have shown nearly stoichiometric $LiVSe_2$ to directly intercalate a range of alkyl amines,[13] though these intercalates were observed over significantly larger timespans than were used in the present work. Interestingly, solvation of fully delithiated VS_2 is observed in both the hexylamine and polyetheramine series, suggesting these may coordinate directly to the anionic VS_2 layers. Aminodecane

does not appear to react to VS_2 despite being chemically and structurally similar to hexylamine. This may be due to the larger aminodecane molecule being too bulky to solvate VS_2 in the timeframe used in these experiments.

A simplified kinetics study was performed on VS_2 for aminodecane and polyetheramine in which the oxidized samples were saturated with either amine for 72 hours. XRD patterns for these experiments are presented in Figure 20. It can be seen that polyetheramine completely converts VS_2 to a solvated phase over an extended time period, while aminodecane does indeed begin to solvate VS_2 given sufficient time. This indicates that solvent properties dictate the rate and extent of solvation to some degree, even in VS_2 samples which are apparently devoid of interlayer cations.

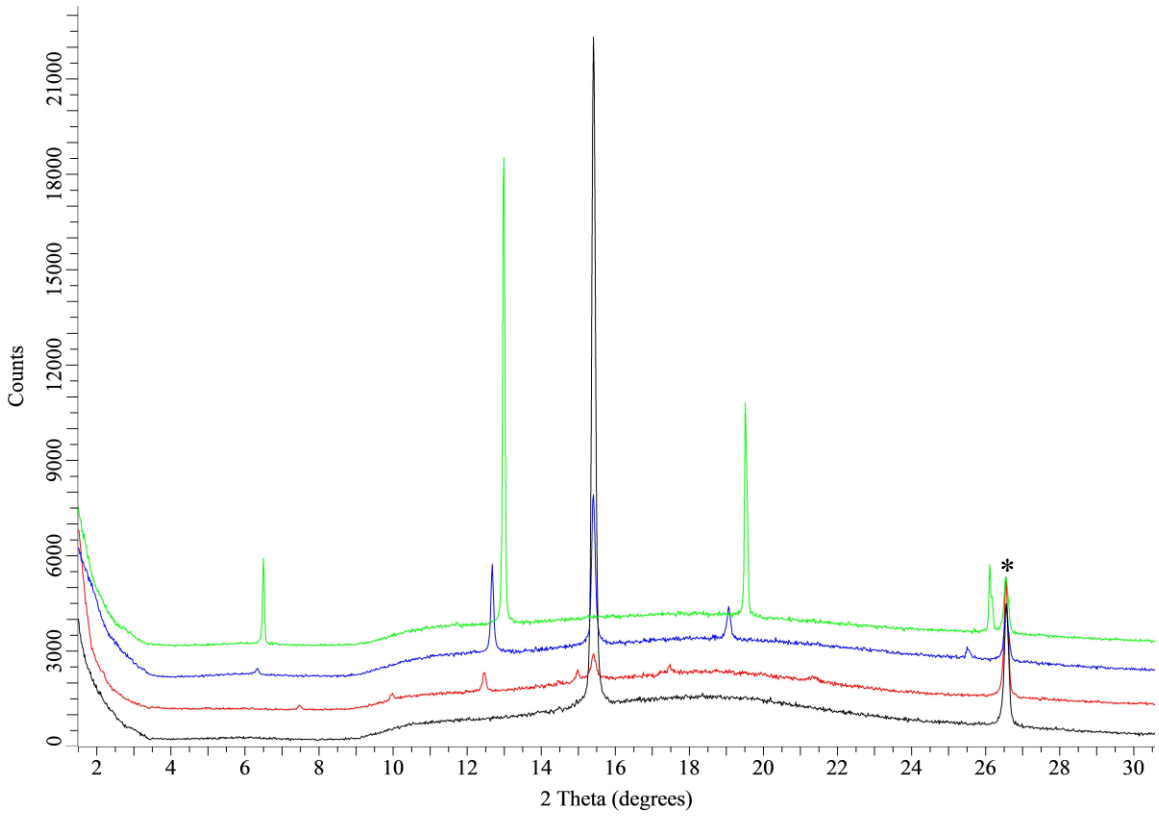

Figure 20. Solvation of VS_2 by aminodecane and polyetheramine. Aminodecane phases measured immediately after exposure (black) and after 72 hours (red). Polyetheramine (EDR-148) phases measured immediately after exposure (dark blue) and after 72 hours (bright green). Graphite denoted by asterisk (*).

It should also be noted that in some early experiments, natively synthesized Li_xVS_2 was found to solvate with DMF to a greater extent than chemically reduced and re-oxidized $Li_{0.8}VS_2$. This is relevant as the stoichiometric lithium content of the as-synthesized compound was determined to be greater than $Li_{0.77}VS$. It seems unlikely this small difference in cation density would affect a substantial difference in solvating character, given the gradual changes observed more recently in this stoichiometric range.

It is possible that a small fraction of vanadium atoms can migrate to the interlayer gallery normally occupied by lithium cations, effectively 'pinning' the layers in that region due to covalent interactions. This migration may be induced by forcibly intercalating additional lithium, pinning the layers at random intervals and frustrating bulk solvation at higher lithium content. It is also possible this behavior is merely due to physical differences in the materials. During the steps involving chemical reduction, a substantial amount of fine silt was removed from the bulk material through subsequent washes. The removal of this fine silt fraction may have selectively altered the solvating character of the bulk sample. Differences observed in solvation character may be due to the presence of smaller crystallites in the as-synthesized material, or even defects introduced by chemical reduction and oxidation.

VII. CONCLUSIONS

A qualitative assessment of all of the XRD data presented here for Li_xVS_2 reveals that stoichiometric $LiVS_2$ does not react with acetonitrile, the N-methyl formamides or primary amines selected. Stoichiometric fractions above 0.8 in Li_xVS_2 do not generally allow significant solvation to occur. Also, the relative intensities of solvated phases are higher at stoichiometric lithium contents below $Li_{0.4}VS_2$. A relationship between the phase diagram of Li_xVS_2 and the degree of solvation can be made. Formamide is seen to form two solvated phases, with an observed shift in abundance between these phases below $Li_{0.4}VS_2$. One can refer back to the phase diagram for Li_xVS_2 (Figure 8) where the β and α phases are both present in this region but separate in lithium fractions above or below this.

From these observations it is apparent that sufficiently coordinating Lewis bases will intercalate the lithium deficient phases, likely coordinating to the remaining lithium cations. No reaction is seen to take place in the 3s phase of $LiVS_2$ during oxidation. Both α and β phases appear to solvate under suitable conditions, where the α-phase appears to solvate more readily. Some Lewis bases are able to solvate the β phase, overcoming the larger cation density and Van der Waals interaction between layers.

Understanding these solvation mechanics may facilitate the use of layered sulfides as high performance battery electrodes. Layered sulfides offer several potential advantages in this regard, such as improved redox cycling, high energy density, and access to relatively plentiful low cost materials. Solvation evidenced by interlayer expansion may only occur in a small fraction of the bulk compound. However as we

have observed it does occur conclusively, and is likely a major factor in expansion of the layered materials when redox occurs in the presence of a suitable Lewis base. Ultimately, an understanding of when and how such solvents intercalate may allow for the design of electrolyte compositions that mitigate damaging volume changes to the electrode over repeated charge cycles.

REFERENCES

[1] Whittingham, M. Stanley, and Russell R. Chianelli. "Layered Compounds and Intercalation Chemistry: An Example of Chemistry and Diffusion in Solids." *Journal of Chemical Education* 57, no. 8 (1980): 569.

[2] Geim, A. K., and K. S. Novoselov. "The Rise of Graphene." *Nat Mater* 6, no. 3 (March 2007): 183–91. doi:10.1038/nmat1849.

[3] Feng, Jun, Xu Sun, Changzheng Wu, Lele Peng, Chenwen Lin, Shuanglin Hu, Jinlong Yang, and Yi Xie. "Metallic Few-Layered VS_2 Ultrathin Nanosheets: High Two-Dimensional Conductivity for In-Plane Supercapacitors." *Journal of the American Chemical Society* 133, no. 44 (November 9, 2011): 17832–38. doi:10.1021/ja207176c.

[4] Kim, Youngsik, Kyu-sung Park, Sang-hoon Song, Jiantao Han, and John B. Goodenough. "Access to M^{3+}/M^{2+} Redox Couples in Layered $LiMS_2$ Sulfides (M = Ti, V, Cr) as Anodes for Li-Ion Battery." *Journal of The Electrochemical Society* 156, no. 8 (2009): A703. doi:10.1149/1.3151856.

[5] Stephenson, Tyler, Zhi Li, Brian Olsen, and David Mitlin. "Lithium Ion Battery Applications of Molybdenum Disulfide (MoS_2) Nanocomposites." *Energy Environ. Sci.* 7, no. 1 (2014): 209–31. doi:10.1039/C3EE42591F.

[6] Voiry, Damien, Maryam Salehi, Rafael Silva, Takeshi Fujita, Mingwei Chen, Tewodros Asefa, Vivek B. Shenoy, Goki Eda, and Manish Chhowalla. "Conducting MoS_2 Nanosheets as Catalysts for Hydrogen Evolution Reaction." *Nano Letters* 13, no. 12 (December 11, 2013): 6222–27. doi:10.1021/nl403661s.

[7] Lukowski, Mark A., Andrew S. Daniel, Fei Meng, Audrey Forticaux, Linsen Li, and Song Jin. "Enhanced Hydrogen Evolution Catalysis from Chemically Exfoliated Metallic MoS_2 Nanosheets." *Journal of the American Chemical Society* 135, no. 28 (July 17, 2013): 10274–77. doi:10.1021/ja404523s.

[8] Mizushima, K., P. C. Jones, P. J. Wiseman, and John B. Goodenough. "Li_xCoO_2 ($0 < x < -1$): A New Cathode Material for Batteries of High Energy Density." *Materials Research Bulletin* 15, no. 6 (1980): 783–89.

[9] Joensen, Per, R. F. Frindt, and S. Roy Morrison. "Single-Layer MoS 2." *Materials Research Bulletin* 21, no. 4 (1986): 457–61.

[10] Murphy, D. W., J. N. Carides, F. J. Di Salvo, C. Cros, and J. V. Waszczak. "Cathodes for Nonaqueous Lithium Batteries Based on VS_2." *Materials Research Bulletin* 12, no. 8 (1977): 825–30.

[11] Whittingham, M. Stanley. "The Electrochemical Characteristics of VSe_2 in Lithium Cells." *Materials Research Bulletin* 13, no. 9 (1978): 959–65.

[12] Dalard, F, D Deroo, A Sellami, R Mauger, and J Mercier. "$VSe_{2-x}S_x$ Materials as Battery Cathode." *Solid State Ionics* 2, no. 4 (November 1981): 321–29. doi:10.1016/0167-2738(81)90034-5.

[13] Guzman, R, J Morales, and J Tirado. "Lithium Solvation by N-Alkylamines in the Interlayer Space of Vanadium Diselenide." *Solid State Ionics* 67, no. 1–2 (December 1993): 107–13. doi:10.1016/0167-2738(93)90315-T.

[14] Evans, John S. O., Stephen J. Price, Heng-Vee Wong, and Dermot O'Hare. "Kinetic Study of the Intercalation of Cobaltocene by Layered Metal Dichalcogenides with Time-Resolved in Situ X-Ray Powder Diffraction." *Journal of the American Chemical Society* 120, no. 42 (October 1998): 10837–46. doi:10.1021/ja9819099.

[15] Coleman, J. N., M. Lotya, A. O'Neill, S. D. Bergin, P. J. King, U. Khan, K. Young, et al. "Two-Dimensional Nanosheets Produced by Liquid Exfoliation of Layered Materials." *Science* 331, no. 6017 (February 4, 2011): 568–71. doi:10.1126/science.1194975.

[16] Smith, Ronan J., Paul J. King, Mustafa Lotya, Christian Wirtz, Umar Khan, Sukanta De, Arlene O'Neill, et al. "Large-Scale Exfoliation of Inorganic Layered Compounds in Aqueous Surfactant Solutions." *Advanced Materials* 23, no. 34 (September 8, 2011): 3944–48. doi:10.1002/adma.201102584.

[17] Novoselov, K. S. "Electric Field Effect in Atomically Thin Carbon Films." *Science* 306, no. 5696 (October 22, 2004): 666–69. doi:10.1126/science.1102896.

[18] Nicolosi, V., M. Chhowalla, M. G. Kanatzidis, M. S. Strano, and J. N. Coleman. "Liquid Exfoliation of Layered Materials." *Science* 340, no. 6139 (June 21, 2013): 1226419–1226419. doi:10.1126/science.1226419.

[19] Murphy, D. Wo, C. Cros, Fr J. Di Salvo, and J. V. Waszczak. "Preparation and Properties of Li_xVS_2 ($0 \leq X \leq 1$)." *Inorganic Chemistry* 16, no. 12 (1977): 3027–31.

[20] Gupta, Asha, C. Buddie Mullins, and John B. Goodenough. "Electrochemical Probings of $Li_{1+x}VS_2$." *Electrochimica Acta* 78 (September 2012): 430–33. doi:10.1016/j.electacta.2012.06.020.

[21] Murphy, D.W., F.J. Di Salvo, and J.N. Carides. “Vanadium Disulfide: Metal Substitution and Lithium Intercalation.” *Journal of Solid State Chemistry* 29, no. 3 (September 1979): 339–43. doi:10.1016/0022-4596(79)90190-7.